Stimulatory MAIT cell antigens reach the circulation and are efficiently metabolised and presented by human liver cells

Martin Lett[1]*, Hema Mehta[2]*, Adrian Keogh[3‡], Tina Jaeger[1‡], Maxime Jacquet[1‡], Kate Powell[2], Marie-Anne Meier[4,5], Isabel Fofana[4], Hassan Melhem[6], Jürg Vosbeck[7], Gieri Cathomas[8], Andres Heigl[9], Markus Heim[4,5], Emanuel Burri[10], Kirsten D. Mertz[8], Jan Hendrik Niess[5,6], Otto Kollmar[11], Christoph J. Zech[12], Robert Ivanek[13,14], Urs Duthaler[15], Paul Klenerman[2,16], Deborah Stroka[3], Magdalena Filipowicz Sinnreich[1,10]

[1] Liver Immunology, Department of Biomedicine, University Hospital Basel and University of Basel, Switzerland
[2] Peter Medawar Building for Pathogen Research, University of Oxford, UK
[3] Department of Visceral Surgery and Medicine, Inselspital, Bern University Hospital, University of Bern, Switzerland
[4] Hepatology, Department of Biomedicine, University Hospital Basel and University of Basel, Switzerland
[5] Division of Gastroenterology and Hepatology, Clarunis, University Center for Gastrointestinal and Liver Diseases, Basel, Switzerland
[6] Gastroenterology, Department of Biomedicine, University Hospital Basel and University of Basel
[7] Institute of Medical Genetics and Pathology, University Hospital Basel, Switzerland
[8] Institute of Pathology, Cantonal Hospital Basel-Land, Liestal, Switzerland.
[9] Department of Surgery, Cantonal Hospital Basel-Land, Liestal, Switzerland
[10] Department of Gastroenterology and Hepatology, Basel University Medical Clinic, Liestal, Switzerland
[11] Division of Visceral Surgery, Clarunis, University Center for Gastrointestinal and Liver Diseases, Basel, Switzerland
[12] Radiology and Nuclear Medicine, University Hospital Basel and University of Basel, Switzerland
[13] DBM Bioinformatics Core Faciliy, Department of Biomedicine, University Hospital Basel and University of Basel, Switzerland
[14] DBM Bioinformatics Core Faciliy, Swiss Institute of Bioinformatics, Basel, Switzerland
[15] Clinical Pharmacology, Department of Biomedicine, University Hospital Basel and University of Basel
[16] Oxford NIHR Biomedical Research Centre, The John Radcliffe Hospital, Oxford, UK

* These authors contributed equally to the manuscript
‡ These authors contributed equally to the manuscript

Table of content

Lett MJ, *et al. Gut* 2022;0:1–13. doi: 10.1136/gutjnl-2021-324478

SUPPLEMENTAL MATERIALS AND METHODS

Unless stated otherwise, all chemicals were received from Merck, Darmstadt, Germany.

Preparation of primary cells from human samples

For isolation of liver cell subsets, a wedge of encapsulated liver was perfused according to the protocol published by Portmann et al.(1) Hepatocytes were isolated by performing consecutive 50 x g centrifugation steps. Isolated hepatocytes were seeded (7 x 10^4 cell/cm^2) onto tissue culture plastic coated with rat tail collagen and were maintained in arginine-free Williams E medium, supplemented with insulin (0.015 IU/ml; Actrapid, Novo Nordisk Pharma, Switzerland), hydrocortisone (5 µm), penicillin / streptomycin (P/S; 100 IU per ml / 100 µg per ml), L-glutamine (2 mM; BioConcept, Allschwil, Switzerland), and ornithine (0.4 mM). 10% FCS (BioConcept) was added to the medium for 12 h following cell plating. After 12 h, medium was exchanged for medium lacking FCS and hepatocyte culture purity was assessed by microscopy; cells were then used for experiments. Brightfield microscopy of primary liver cells was performed on the Olympus IX81 microscope. IF staining of hepatocytes was performed using antibody against HNF-4α. Fluorescence images of primary cell populations were taken on the Nikon Ti2 microscope (Nikon, Tokyo, Japan).

Hepatic myofibroblasts/stellate cells (HSCs) were isolated by outgrowth from a suspension of liver derived non-parenchymal cells (NPCs), the fraction previously deprived of hepatocytes, plated in DMEM high glucose supplemented with 20% FCS, P/S, L-glutamine, 1 mM pyruvate, and Non-Essential Amino Acid (NEAA; BioConcept). After 24 h, the attached cells were washed once with PBS and cultured for additional 7 days. Mainly HSCs outlast this selection; their purity was assessed by FACS using their strong autofluorescence (due to Vitamin A storage) at λ=400-500 nm (violet channel) as readout, and by immunofluorescence (IF) staining using Ab against alpha-smooth muscle actin.

Isolation of Liver sinusoidal endothelial cells (LSECs) was carried out by positive immunomagnetic selection, according to the protocol of Shetty et al.(2) using a CD31 Ab conjugated to DYNABEADS (Thermo Fisher Scientific, Waltham (MA), USA). We use the term LSECs throughout the manuscript, although this protocol will yield not only endothelial cells of

sinusoidal origin, but also endothelial cells originating from the liver vasculature, the latter possibly contributing to Ag presentation by LSECs to MAIT cells. The cells were maintained in endothelial cell basal medium containing 10% human AB^+ serum (obtained from the blood donation centre, Basel, Switzerland), hepatocyte growth factor (10 ng/ml; PeproTech, Rocky Hill, NJ, USA), vascular endothelial growth factor (10 ng/ml; PeproTech), P/S, L-glutamine, pyruvate, and NEAA. The cells were grown in collagen-coated tissue culture plastic dishes. Identity of LSECs/endothelial cells were assessed by IF microscopy using a CD31 Ab, confirming the effectiveness of the isolation method.

Isolation of biliary epithelial cells (BECs) was performed by positive selection using EpCAM according to the protocol published previously.(3) BECs were maintained in epithelial cell medium composed of a 1:1 mix of DMEM low glucose and DMEM/F12-ham (Thermo Fisher), supplemented with 10% FCS, P/S, adenine (18 µM), insulin (0.15 U/ml Humalog®, Eli Lilly SA, Switzerland), epinephrine (1 mg/ml), triiodothyronine-transferrin (1.1 µg/ml; 8.2 µg/ml), epidermal growth factor (10 ng/ml, PeproTech, Rocky Hill, NJ, USA), and hydrocortisone (13.4 µg/ml). BECs were assessed by IF microscopy using Ab against CK19.

Adipocyte stromal cells (ASCs) were obtained from adipose tissue as described,(4) and kindly provided to us by Prof. Arnaud Scherberich. Their differentiation into adipocytes was performed in 2D cultures as previously described.(5) In brief, cells were cultured in alpha-MEM with 10% FBS until they reached confluency. Medium was then supplemented with 10 µg/ml insulin, 10 µM dexamethasone, 100 µM indomethacin and 500 µM 3-isobutyl-1-methyl xanthine (adipogenic induction medium) for 2 weeks and thereafter with 10 µg/ml insulin (adipogenic maintenance medium) for 1 week.

HUVEC cells were isolated from umbilical cord as described by Crampton et al. and maintained in endothelial cell basal medium supplemented as described for LSECs.(6)

Buffy coats for isolation of peripheral blood mononuclear cells (PBMCs) were obtained at the blood donation center in Basel. PBMCs were isolated by density gradient centrifugation on Ficoll (Lymphoprep®; Axonlab, Baden, Switzerland), using a standard protocol.(7)

Immunofluorescence (IF) and immunohistochemistry (IHC) staining of human liver sections and analysis of cell distribution

Cryo-sections (from OCT-embedded liver samples) of 8 µm thickness were mounted on microscopy slides and fixed in 4% formaldehyde for 10 min at room temperature (RT). Slides were then washed twice for 10 min in PBS and blocked in blocking buffer [1% Normal donkey serum (Jackson Immuno Research, Ely, UK), 2% fish gelatine, 0.15% Triton-X-100 in PBS] for 1 h at RT. Slides were incubated with primary Abs, diluted in blocking buffer, at 4°C overnight, washed with PBS, and then incubated with secondary Abs at RT for 1 h. After washing with PBS, slides were mounted in mounting solution containing 300 µM DAPI. Abs used were anti-IL-18Rα, anti-TCR Vα7.2 and anti-CD3. Secondary Abs were donkey-anti-goat-Cy3, donkey-anti-mouse-A488, and donkey-anti-rabbit-A647. Fluorescence images were taken on the Olympus BX63 microscope (Olympus, Tokyo, Japan) and the Nikon Ti2, using the 20x objective, and analysed with Image J (https://fiji.sc/) and QuPath.(8, 9)

For the chip cytometry, cryo-sections were cut directly onto APES-coated coverslips and stored frozen at -80°C. Sections were fixed with ice-cold acetone for 5 minutes, washed in cold PBS and assembled into tissue chips (Zellsafe Tissue chips, Zellkraftwerk, Germany) which were immediately filled with PBS or storage buffer (Zellkraftwerk, Germany). Staining was performed using a previously validated protocol.(10) Briefly, sections were blocked with 5% normal goat serum (Thermo Fisher) in PBS for at least one hour at room temperature. Immunostaining was performed using fluorophore-conjugated primary antibodies at room temperature for 30 minutes (CD3, Vα7.2, IL18R-α, CD161, CD4, and CD8). Antibody cocktails were diluted in PBS alone or PBS containing 2% BSA or 2% normal goat serum. Iterative rounds of staining and bleaching were used to build up multiplex panels.

Paraffin embedded sections of healthy liver tissues were used for visualization of NK cells, defined as $CD57^+$ $CD3^-$ cells. The staining protocol was described by Correia et al.(11) Briefly, for double staining of CD3 and CD57, a BOND-III fully automated stainer and BOND kits (Leica Biosystems) were used. Slides were pre-treated with EDTA buffer for 20 min at 100 °C, stained with rabbit anti-CD3 for 15 min at RT, and then with the BOND Polymer

Refine Red Detection (Leica) kit. After CD3 staining, mouse anti-CD57 was applied for 15 min at RT, and revealed with the BOND Polymer Refine Detection kit (Leica). Counterstaining was performed with hematoxylin for 5 min.

Cell detection and calculation of distance to regions of interest (ROIs) within liver biopsy and liver resection images was performed using QuPath. Briefly, a ROI was drawn around the liver tissue and its total surface measured. The StarDist deep-learning-based method of 2D and 3D nucleus detection was used for cell detection within the tissue.(12) The positivity for CD3, TCR Vα7.2 and IL-18Rα staining was assessed manually and cells were classified into single ($CD3^+$), double ($CD3^+$ TCR $V\alpha7.2^+$) or triple positive ($CD3^+$ TCR $V\alpha7.2^+$ IL-$18R\alpha^+$). Liver structures were evaluated using H&E staining of consecutive sections associated with the IF stained tissues to annotate the central veins and portal fields. Using the "distance to annotation 2D" spatial analysis tool, we calculated the distance of single or triple positive classified cells to the ROI annotations. Only liver biopsies/resection specimen with an intact structure and presenting enough ROIs were used for distance calculations. For the MAIT cell distribution analysis, we analyzed 9 samples (4 biopsies, 5 resection specimen) with a total of 121 portal fields and 109 central veins. Accordingly, $CD57^+$ $CD3^-$ cells were assigned manually for the analysis of NK cell distribution. For the NK cell distribution analysis, we analyzed 11 samples (4 biopsies, 8 resection specimen) with a total of 287 portal fields and 272 central veins. Measurement data were imported into CytoMAP, a MatLab toolbox, to create a heatmap visualization of the distance to the closest MAIT cell, non-MAIT T cell or NK cell.(13) In total, for the MAIT cell distribution shown in fig. 2D, 1,838 MAIT cells and 10,184 non-MAIT T cells were analyzed. For NK cell distibution, shown in Supplemental Fig. 1E, 582 NK cells and 7,999 T cells (including MAIT cells) were analyzed.

Cell lines and MAIT cell clones

All cell lines used are listed in supplemental Table 2. LX2 cells were cultured in DMEM high glucose, and HepG2 and Huh7 cells in DMEM low glucose, supplemented with 10% FCS, P/S, L-glutamine, pyruvate and NEAA. TMNK-1 and TWNT-4 cell lines were grown in DMEM GlutaMax™ (Thermo Fisher) with P/S, pyruvate and NEAA. K562 and THP-1 cells were

cultured in RPMI 1640 containing 10% FCS, P/S and L-glutamine, pyruvate, with or without NEAA, depending on the experiment. All cells were grown at 37°C under 5% CO_2 atmosphere.

In order to generate the K562-MR1 cell line, we transduced K562 cells with a lentivirus coding for human MR1 covalently linked with β2M; this construct was generously provided by Prof. Gennaro De Libero, Department of Biomedicine, University Hospital Basel, Switzerland.(14) We confirmed MR1 overexpression and cell surface display by flow cytometry, after staining the cells with mouse-anti-MR1 (clone 26.5; monoclonal Ab purified from a hybridoma kindly provided by Prof. Marina Cella, Washington University School of Medicine, St. Louis).(15)

Human MAIT cell clone SMC3 was also kindly provided by Prof. Gennaro De Libero.(6) This clone was generated from the peripheral blood of a healthy donor. In brief, sorted MAIT cells were cloned by limiting dilution using PHA (1 µg/ml), human IL-2 (100 IU/ml) and irradiated PBMCs (5×10^5/ml). The SMC3 MR1-restricted T cell clone was cultured and re-stimulated periodically as described by Lepore et al,(16) and maintained in complete RPMI-1640 medium containing 5% AB^+ human serum, and 100 IU/ml IL-2.

Non-parenchymal cells (NPCs) obtained from normal liver tissue samples of two patients undergoing surgery for colorectal cancer metastasis were used to generate two liver-derived MAIT cell lines, designated MAIT-BEL-10 and MAIT-BSL-19. The NPC fraction was obtained after perfusion of the liver wedge with “collagenase buffer” (684 mM NaCl, 13 mM KCl, 3 mM Na_2PO_4 $2H_2O$, 125 mM HEPES, 25 mM $CaCl_2$; pH 7.4; containing 200 IU/ml collagenase type IV), and low speed centrifugation to deplete hepatocytes (see details further above). Liver-associated mononuclear cells were isolated by density gradient centrifugation on Ficoll. MAIT cells were then FACS-sorted based on expression of CD3 and staining by MR1 Tetramer and expanded by stimulation with phytohemagglutinin (PHA) and human IL-2 (100 IU/ml) in the presence of irradiated peripheral blood mononuclear cells (PBMCs) (40 Gray) as feeder cells. MAIT cells were maintained in RPMI 1640 medium supplemented with 5% AB^+ human serum, IL-2 (100 IU/ml), Penicillin/Streptomycin (100 IU/ml; P/S), L-glutamine, pyruvate and non-essential amino acids (NEAA).

Preparation of bacterial products and synthetic MAIT cell Ag

Synthetic Ag 5-(2-oxopropylideneamino)-6-D-ribitylaminouracil (5-OP-RU) was generated according to the protocol published by Corbett et al.(17) In brief, Ag precursor 5-amino-6-D-ribitylaminouracil (5-A-RU; Toronto Chemicals, Canada) was mixed with 10 molar equivalents of methylglyoxal and incubated for 5 min on ice. The resulting 5-OP-RU was used immediately upon preparation to prevent its transformation into 7-Hydroxy-6-methyl-8-ribityl lumazine (RL-6-Me-7-OH) or 7-methyl-8-D-ribityllumazine (see supplemental fig. 8A).

Fixed bacteria: *E. coli* (DH5α) was grown on lysogenic broth (LB) agar plates for 16 h at 37°C before fixing in 2% paraformaldehyde (PFA) for 20 min followed by several PBS washing steps. Before fixation, bacteria were plated to determine the number of colony forming units (CFUs). Concentration-adjusted stocks of fixed bacteria were re-suspended in PBS.

E. coli lysate: The DH5α strain was grown in LB medium. Cells were harvested during exponential growth and washed three times with cold 0.9% NaCl. Before the last wash, an aliquot was removed to determine the CFU. The pellet was subsequently resuspended in 70% ethanol and the cells were disrupted by two consecutive French press rounds. After centrifugation (15,000 x g for 20 min at 4°C), supernatant was lyophilized overnight and the concentration was adjusted to an equivalent of 5 x 10^{11} CFU/ml. The lysate was stored at -80°C.

Ag presentation assays

In Ag presentation assays with established cell lines (shown in fig. 2 and supplemental fig. 2), the cells were co-cultured, unless indicated otherwise, with isolated blood-derived $CD8^+$ T cells at a ratio of 1:4, in 96 well flat bottom plates. Synthetic Ag 5-OP-RU or fixed *E. coli* were added at the concentration (CFU/ml) indicated, followed by 16 h incubation at 37°C. Brefeldin A and Monensin (both from BioLegend, San Diego, USA) were added for the final 4 h of incubation. $CD8^+$ T cells were subjected to FACS analysis.

All assays with primary liver cell subtypes and also non-liver primary cells used as APCs were performed in RPMI medium containing 10% FCS (always the same lot number)

and supplemented as described above to exclude nonspecific effects of variable cell media. APCs were seeded and kept for 4 h at 37°C to allow for attachment/adaptation. Following this, *E. coli* lysate or synthetic Ag was added at indicated concentration and cells were incubated for 2 h prior to the addition of MAIT cells, at an APC to MAIT cell ratio of 1:4. Primary MAIT cells were used right after isolation, and the MAIT cell clone SMC3 as well as the liver-derived MAIT cell lines at day 14 after re-stimulation. MAIT cell activation as well as cytokine secretion was evaluated after 16 h of co-culture.

To perform blocking experiments, cells were incubated with Ag and the corresponding blocking Abs (10 µg/ml anti-MR1, 5 µg/ml anti-IL-12 or 4 µg/ml anti-IL-18) were added after 1 h, followed by a 1 h incubation step before the addition of MAIT cells. To test the blocking potential of non-activating MR1 ligands, 6-formylpterin (6-FP; 50 µM), acetyl-6-FP (5 µM) or 20 - 100 µM 5-formyl-salicylic acid (5-F-SA) was added 1 h before the addition of 5-OP-RU.

Quantitative Real-Time PCR (RT-qPCR)

RNA was purified from primary liver cell types with Nucleo Spin RNA II kit (Macherey-Nagel, Düren, Germany) according to manufacturer's instructions. RNA was reverse transcribed by Moloney murine leukemia virus reverse transcriptase (Promega Biosciences, Wallisellen, Switzerland) in the presence of random Primers (Promega) and deoxynucleoside triphosphates, according to manufacturer's instructions. All reactions were performed in triplicates on an ABI 7500 Real-Time PCR System (Applied Biosystems, Faster City (CA), USA) using SYBR green fluorescence (FastStart Universal SYBR® green; Roche, Basel, Switzerland) as read out. mRNA expression levels of the MR1 transcript were normalized to GAPDH mRNA or 18S rRNA levels using the ΔCt method. The primers were designed across exon-intron junctions to prevent contribution from genomic DNA amplification (MR1_F: 5'-TGC GGTGTCCACATGGTTCT-3', MR1_R: 5'-TTTGCTCTCGGGGCCTTCT-3'; GAPDH_F: 5'-AAGTATGACAACAGCCTCAAGAT-3', GAPDH_R: 5'-CATGAGTCCTTCCACGATACC-3'). The 18S rRNA primers were: F, 5'-GCTTAATTTGACTCAACACGGGA-3' and R, 5'-AGCTATCAATCTGTCAATCCTGCT-3'.

Enzyme-linked immunosorbent assay (ELISA)

For the ELISA, analysis plates (Maxisorp, NUNC, Thermo Fisher) were coated overnight at 4°C with 2.5 µg/ml capture Ab for IFN-γ (Clone MD-1) or IL-17A (Clone BL-23). The next day, unspecific sites were blocked with 0.5% fractionated gelatine for 1 h at RT. The samples were incubated for 2 h, followed by 1 h incubation step with biotinylated Ab, either 1 µg/ml anti-IFN-γ or 0.3 µg/ml anti-IL-17A, and 1 h incubation with either 0.25 µg/ml Streptavidin-HRP (BioLegend) for the IFN-γ or 0.1 µg/ml Streptavidin-PolyHRP80 (SDT GmbH, Baesweiler Germany) for the IL-17A ELISA. Between each step, the plate was rinsed 3 times with PBS 0.05% Tween. Revealing was performed after incubation with OPD (SIGMAFAST™) by reading absorbance at λ=490 nm.

Flow cytometry analysis

For the intracellular staining, cells were washed with PBS and stained with Live/Dead Cell Stain (Thermo Fisher) for 15 min, followed by a 10 min fixation step with 4% PFA prior to permeabilizing the cells for 10 min. Cells were then incubated with the Ab cocktail (see supplemental Table 3) for 20 min before washing and re-suspending in PBS for analysis on MACSQuant analyzer (Miltenyi Biotech, Bergisch Gladbach, Germany).

For the surface staining, mononuclear cells were washed in PBS and stained with Live/Dead® Fixable Dead Cell Stain blue (Thermo Fisher), and rinsed once in staining buffer (PBS with 0.5% human albumin and 3 mM sodium azide), followed by incubation with Abs against cell-surface molecules. For the CD107a staining, anti-human CD107a antibody and monensin (2 µM) were added to the culture directly after the addition of the T cells, such that the cells were continuously stained during the overnight incubation period. Data were acquired on the LSRFortessa™ (BD Biosciences, Allschwil, Switzerland) equipped with 5 lasers (355, 405, 488, 561, and 640 nm) and 18 filters, or the Aurora (Cytek, Amsterdam, Netherlands) also with the same 5 lasers and 60 channels (full spectrum cytometry), unmixed with SpectroFlo® when necessary, and analysed with FlowJo 10.0.7 (TreeStar, Ashland, OR, USA). After excluding doublets and DAPI- or LIVE/DEAD stain-positive cells, MAIT cells were identified as

CD3+CD161highVα7.2+ and/or MR1 tetramer (APC-labeled MR1 5-OP-RU tetramer; NIH Tetramer Core Facility, Emory University, Atlanta, GA, USA) positive cells.

Mass spectrometry analysis

5-OP-RU was analysed in cell extracts and cell supernatants by liquid chromatography (LC; Shimadzu, Kyoto, Japan) tandem mass spectrometry (MS/MS: API 4000, AB Sciex, Concor, Canada). A Synergi Polar-RP analytical column (Phenomenex, Torrance, USA) was used as the stationary phase, while the mobile phase consisted of water (mobile A) and methanol (mobile B), both supplemented with 0.1% acetic acid. 5-OP-RU eluted at 2.14 min when using the following gradient program: 0 - 0.5 min 20% B, 0.5 - 1.5 min 20-95% B, 1.5 - 2.5 min 95% B, 2.5 - 3 min 20% B. The sample was online diluted during the first 0.5 min with mobile phase A via a t-union, which was connected in front of the analytical column. The flow rate was kept constant (0.8 ml/min). Aliquots of cell supernatant (50 µl) or cell extract (from 1.5 million cells) were extracted with 150 µl 100% methanol and 200 µl 75% methanol, respectively. After centrifugation, supernatants (20 µl) of extracts were injected into the LC-MS/MS system. 5-OP-RU was analysed by electrospray ionization and selected reaction monitoring in the negative mode using the mass transition 329.0 m/z → 190.9 m/z (declusting potential: -110 V, entrance potential: -10V, collision energy: -24 V, collision cell exit potential: -9 V, gas: N2). Analyst software 1.6.2 (AB Sciex, Concord, Canada) was used to analyse the data and to operate the LC-MS/MS system.

Measurement of antigenic potential of human serum

For Ag presentation assays using human serum, 10^4 K562-MR1 cells were seeded in RPMI medium without FCS and 50 µl of human serum was added. In experiments testing inhibition by acetyl-6-FP, K562-MR1 cells were incubated with 5 µM acetyl-6-FP for 1 h before the serum addition. After 2 h incubation with serum, 35 µg/ml anti-MR1 Ab was added when indicated, followed by 1 h incubation before the addition of 5 x 10^4 SMC3 MAIT cells and further incubation for 16 h. IFN-γ was measured by ELISA using 6 µg/ml IFN-γ capturing antibody,

0.6 µg/ml biotinylated secondary antibody, and revealed with 0.1 µg/ml Streptavidin-PolyHRP80 (SDT GmbH, Baesweiler, Germany). To calculate 5-OP-RU equivalents, control MAIT cell activation assays containing different concentrations of 5-OP-RU (0.006-25 pM) were included in each plate used to test human sera.

For assays measuring intracellular IFN-γ staining in MAIT SMC3 cells (supplemental fig. 9A-C), experimental conditions were similar to those used for ELISA assays, except that final incubation after the SMC3 MAIT cells addition was for 7 h in presence of 5 µg/ml Brefeldin A. In control experiments, 5-OP-RU (0.1-10 pM) was added instead of the human serum. IFN-γ positive MAIT cells were assessed by FACS.

D-lactate assay

Serum D-lactate levels were measured with the colorimetric D-lactate assay (Abcam, Cambridge, UK). Deproteinization of the serum samples was carried out with 10 kD spin columns (Corning, New York, USA). In brief, 400 µl of the serum was added to the spin columns and centrifuged at 4°C for 30 min at 12,000 x g, the flow-through was analyzed according to the manufacturer's instructions.

Lett MJ, *et al. Gut* 2022;0:1–13. doi: 10.1136/gutjnl-2021-324478

SUPPLEMENTAL TABLES

Supplemental Table 1. Key resources

Reagent or Material	Supplier	Identifier Cat#
Growth media / Supplements		
Adenine	Merck, Darmstadt, Germany	A8626
DMEM high glucose	Merck, Darmstadt, Germany	D6571
DMEM low glucose	Merck, Darmstadt, Germany	D5546
DMEM/F12-ham	Thermo Fisher Scientific, Waltham (MA), USA	21331
DMEM GlutaMax™	Thermo Fisher Scientific, Waltham (MA), USA	10569010
Endothelial cell basal medium	Merck, Darmstadt, Germany	210-500
Epidermal growth factor	PeproTech, Rocky Hill (NJ), USA	100-15
Epinephrine	Merck, Darmstadt, Germany	E4250
Foetal Calf Serum, FCS	BioConcept, Allschwil, Switzerland	2-01F10-I
Hepatocyte growth factor	PeproTech, Rocky Hill (NJ), USA	100-39H
Hydrocortisone	Merck, Darmstadt, Germany	H-0888
IL-2, human	PeproTech, Rocky Hill (NJ), USA	200-02
IL-7, human	PeproTech, Rocky Hill (NJ), USA	200-07
Insulin, ACTRAPID®	Novo Nordisk Pharma AG, Zürich, Switzerland	
Insulin, HUMALOG®	Eli Lilly SA, Vernier, Switzerland	VL7394
L-glutamine	BioConcept, Allschwil, Switzerland	5-10K50-H
Non-Essential Amino Acid	BioConcept, Allschwil, Switzerland	5-13K00-H
Ornithine		
Penicillin / Streptomycin	Merck, Darmstadt, Germany	P-4333
Phytohemagglutinin	Thermo Fisher Scientific, Waltham (MA), USA	10082333
RPMI 1640 medium	Merck, Darmstadt, Germany	R0883
Triiodothyronine	Merck, Darmstadt, Germany	T6397
Transferrin	Merck, Darmstadt, Germany	T1147
Vascular endothelial growth factor	PeproTech, Rocky Hill (NJ), USA	100-20
Williams E medium	Merck, Darmstadt, Germany	W4128
Reagents		
5-amino-6-D-ribitylaminouracil	Toronto chemicals, CA	A629245
5-formyl-salicylic acid	Merck, Darmstadt, Germany	F17601
6-Formylpterin	Schircks Laboratories, Jona (SG), Switzerland	11.415
Acetyl-6-Formylpterin	Schircks Laboratories, Jona (SG), Switzerland	11.418
Brefeldin A	BioLegend, San Diego (CA), USA	420601
Casein buffer, biotin-free	SDT GmbH, Baesweiler, Germany	CBC1
Collagen	Merck, Darmstadt, Germany	C3867
Collagenase type IV	Merck, Darmstadt, Germany	C5138
Deoxynucleoside triphosphates	Promega Biosciences, Inc., Wallisellen, Switzerland	U1515
Ficoll, LYMPHOPREP®	Axonlab, Baden, Switzerland	1114547
Fish gelatin	Merck, Darmstadt, Germany	G7041
Fractionated gelatine	Merck, Darmstadt, Germany	37766
Live/Dead Cell Stain Near-IR	Thermo Fisher Scientific, Waltham (MA), USA	L10119
LIVE/DEAD® Fixable Dead Cell Stain blue	Thermo Fisher Scientific, Waltham (MA), USA	L23105
Live-or-Dye™ 350/448	Biotium, Hayward (CA), USA	32018

Methylglyoxal	Merck, Darmstadt, Germany	R0252
Moloney murine leukemia virus reverse transcriptase	Promega Biosciences, Inc., Wallisellen, Switzerland	M1701
Monensin	BioLegend, San Diego (CA), USA	420701
Zombie NIR™ Fixable viability stain	BioLegend, San Diego (CA), USA	423105
Normal donkey serum	Jackson Immuno Research, Ely, UK	017-000-121
o-Phenylenediamine dihydrochloride; SIGMAFAST™ OPD	Merck, Darmstadt, Germany	F4648
Random Primers	Promega Biosciences, Inc., Wallisellen, Switzerland	C1181
Streptavidin-HRP	BioLegend, San Diego (CA), USA	405210
Streptavidin-PolyHRP80	SDT GmbH, Baesweiler, Germany	SP80C
SYBR green; FastStart Universal SYBR® green master	Roche, Basel, Switzerland	28137500
Other		
DYNABEADS™	Thermo Fisher Scientific, Waltham (MA), USA	10007D
D-lactate Assay Kit (Colorimetric)	Abcam, Cambridge, UK	ab83429
ELISA plates; Maxisorp	NUNC / Thermo Fisher Scientific, Waltham (MA), USA	439454
Nucleo Spin RNA II kit	Macherey-Nagel, Düren, Germany	740984
Miltenyi positive selection kit	Miltenyi Biotec, Bergisch Gladbach, Germany	130-096-495
Spin-XR UF 500 µL Centrifugal Concentrator, 10,000 MWCO	Corning, New York, USA	431478

Supplemental Table 2. Cell lines

Name	Description	Source	Reference
H69	SV40 T Ag transformed biliary cell line, derived from normal liver	Douglas Jefferson[1], provided by Christian Fingas[2]	(18)
HepG2 Huh7	Hepatocarcinoma cell lines	American Type Culture Collection	(19, 20)
K562	Chronic myeloid leukemia cell line	American Type Culture Collection	
K562-MR1	K562 cells constitutively expressing MR1-β2M		This study
LX2	SV40 T Ag immortalized stellate cell line	Scott L. Friedman[3]	(21)
MAIT-BEL-10	Liver-derived MAIT cell line		This study
MAIT-BSL-19	Liver-derived MAIT cell line		This study
SMC3	Human MAIT cell clone	Gennaro De Libero[4]	(14)
THP-1	Myelomonocytic leukemia cell line	American Type Culture Collection	
TMNK-1	LSEC cell line	Naoya Kobayashi[5]	(22)
TWNT-4	Stellate cell line	Naoya Kobayashi[5]	(22)

[1]New England Medical Center, Tufts University; [2]University Duisburg Essen, Germany; [3]Icahn School of Medicine at Mount Sinai, New York, USA; [4]Department of Biomedicine, University Hospital Basel, Switzerland; [5]Okayama University, Japan.

Supplemental Table 3. Antibodies

Antibody	Clone	Probe/Fluorophore	Company	Cat#
Antibodies for Enrichment				
CD36	REA760	Biotin	Miltenyi Biotec	130-110-738
TCR γδ	REA591	Biotin	Miltenyi Biotec	130-113-510
CD4	REA623	Biotin	Miltenyi Biotec	130-113-224
CD14	REA599	Biotin	Miltenyi Biotec	130-110-517
CD19	REA675	Biotin	Miltenyi Biotec	130-113-644
CD45RA	REA1047	Biotin	Miltenyi Biotec	130-117-750
Antibody Cocktail used for the intracellular staining (Fortessa)				
CD3	UCHT1	PerCP/Cyanine5.5	BioLegend	300430
CD8	BW135/80	VioGreen	Miltenyi	130-113-164
CD161	191B8	PE	Miltenyi	130-113-593
Vα7.2	3C10	APC	BioLegend	351708
IFN-γ	45-15	FITC	Miltenyi	130-091-641
TNF-α	MAb11	PE/Cyanine7	BioLegend	502930
CD69	FN50	FITC	Invitrogen	11-0699-42
Antibody Cocktail used for the surface staining (Fortessa)				
CD107a	H4A3	FITC	Biolegend	328605
CD8α	RPA-T8	BUV496	BD Biosciences	564804
CD3	UCHT1	BV510	Biolegend	300448
CD161	HP-3G10	BV605	Biolegend	339916
TCR Vα7.2	3C10	BV785	Biolegend	351722
CD279/PD-1	EH12.2H7	PE/Cyanine7	Biolegend	329918
CD137	4B4-1	Alexa Fluor® 700	Biolegend	309816
CD69	FN50	APC/Cyanine7	Biolegend	310914
Antibody Cocktail used for the surface staining (Aurora)				
CD71	M-A712	BUV563	BD Biosciences	749296
CD314	1D11	BUV737	BD Biosciences	748426
CD26	M-A261	BUV805	BD Biosciences	749316
CD107a	H4A3	BV785	Biolegend	328643
CD45	2D1	Spark Blue 550	Biolegend	368549
CD4	OKT4	PerCP	Biolegend	317431
CD279	EH12.2H7	PE/Dazzle™ 594	Biolegend	329939
CD25	M-A251	PE-Fire 640	Biolegend	356148
CD127	A019D5	PE-Fire 700	Biolegend	351366
CD137	4B4-1	APC	Biolegend	309809
CD69	FN50	Alexa Fluor® 700	Biolegend	310921
TCR Vα7.2	3C10	APC/Cyanine7	Biolegend	351713
CD16	3G8	BV570	Biolegend	302035
CD49a	TS2/7	FITC	Biolegend	328308
CD101	BB27	PE	Biolegend	331011
CD25	M-A251	PE/FIRE 640	Biolegend	356148
CD103	Ber-ACT8	PE-Cyanine7	Biolegend	350212
hMR1 5-OP-RU Tetramer	Not applicable	BV421	NIH Tetramer Core Facility Emory University	
CD186 (CXCR6)	K041E5	AF647	Biolegend	356008
Antibodies for Immunofluorescence staining				
α-SMA	1A4		Sigma	5228
CK-19	B170		Leica Biosystems	NCL-CK19
HNF-4α	polyclonal		Santa Cruz	Sc-8987
CD31	WM59	Alexa Fluor® 488	Biolegend	303110
IL-18Rα	polyclonal		R&D System	AF840

TCR Vα7.2	3C10		Biolegend	351702
CD3	polyclonal		DAKO	A0452
Anti-Mouse	polyclonal		Jackson Immuno Research	715-545-150
Anti-Rabbit	polyclonal		Jackson Immuno Research	711-605-152
Anti-Goat	polyclonal		Jackson Immuno Research	705-165-147
CD3	UCHT1	PerCP	Biolegend	300428
CD4	RPA-T4	PE	Biolegend	300508
CD8	SK1	PerCP/Cy5.5	Biolegend	344704
CD161	191B8	PE	Miltenyi	130-114-119
IL-18Rα	H44	PE	Biolegend	313808
TCR Vα7.2	3C10	PE	Biolegend	351706
	Antibodies for IHC staining			
CD57	NK-1		Diagnostic BioSystems	MOB163
CD3	LN10		Leica	NCL-L-CD3-565
	Blocking Antibodies			
IL12/IL23	C8.6		Biolegend	508804
IL-18	125-2h		MBL	D044-3
MR1	26.5	APC	Biolegend	361108

Supplemental Table 4. Patient characteristics of liver and resection biopsy samples used for assessment of MAIT cell localisation in normal human liver by IF staining (see fig. 1 and supplemental fig. 1). The samples in bold were used for computational analysis depicted in fig. 1D.

Patient ID	Age range	% MAIT/ CD3	% Vα7.2$^+$ IL18Rα$^-$/CD3	ALT [U/l]	AST [U/l]	GGT [U/l]	AP [U/l]	Bilirubin [µmol/l]	Reason for biopsy/resection	Biopsy result
C1	30-39	14.33	1.75	88	33	447	111	4	Suspicion of medication induced hepatotoxicity	Liver parenchyma without pathological changes.
C2	40-49	10.95	1.41	35	23	116	71	10	Isolated GGT increase	Liver parenchyma without pathological changes.
C3	50-59	32.97	3.62	91	49	216	204	8	Increased Transaminases/ GGT/AP	Liver parenchyma without pathological changes.
C4	60-69	22.22	1.71	15	22	20	41	12	Calcified liver mass	Liver parenchyma without pathological changes.
C5	50-59	22.9	0.46	43	39	406	150	9	Focal nodular hyperplasia	Liver parenchyma without major pathological changes. Minimal steatosis <10%.
C6	40-49	30.18	3.52	56	24	154	84	21	Increased Transaminases/GGT	Liver parenchyma without major pathological changes. Minimal unspecific lymphocytic infiltrates, minimal sinusoidal dilation.
C7	30-39	8.38	2.23	42	26	137	76	4	Increased Transaminases	Liver parenchyma without major pathological changes. Minimal reactive hepatitis.
C8	20-29	11.9	0.85	21	29	14	62	10	Increased Transaminases (again normal at biopsy)	Liver parenchyma without major pathological changes. Minimal unspecific lobular inflammation.
C9	40-49	17.39	4.35	43	28	202	159	5	Increased Transaminases/ GGT/AP	Liver parenchyma without pathological changes.
C10	40-49	18.67	1.90	40	30	187	162	9	Increased GGT/AP	Liver parenchyma without pathological changes.
C11	40-49	5.43	2.17	43	35	223	78	4	Increased Transaminases/GGT	Liver parenchyma without pathological changes.
C12	50-55	12.97	1.50	16	20	22	53	8	Resection of hemangioma	Liver parenchyma without pathological changes.
C13	20-29	27.53	0.26	36	31	119	130	8	Resection of focal nodular hyperplasia	Liver parenchyma without pathological changes.
C14	70-79	15.21	0.10	18	21	19	58	4	Resection of colorectal cancer metastasis	Liver parenchyma without major pathological changes. Minimal steatosis 5%.
C15	60-69	9.93	0.15	21	22	217	137	3	Resection of anal carcinoma metastasis	Liver parenchyma without major pathological changes. Minimal steatosis <10%.

ALT: Alanine amino-transferase; AST: Aspartate amino-transferase; GGT: γ-glutamyltransferase; AP: Alkaline phosphatase

Supplemental Table 5. Characteristics of patients undergoing TIPSS procedure (see fig. 7 and supplemental fig. 9).

Patient ID	Age range	Gender (m/f)	ALT [U/l]	AST [U/l]	GGT [U/l]	AP [U/l]	Bili-rubin [µmol/l]	Albumin [g/l]	INR	Hb [g/l]	Thrombo-cytes [x 10^9/l]	Reason for TIPSS placement	Time from TIPSS (months)
T1	70-79	m	30	54	159	131	37	37	1.4	104	78	NRH-related portal hypertension, acute-on chronic portal vein thrombosis	0 and 5
T2	50-59	m	19	37	196	154	19	25	1.3	129	119	Child B cirrhosis, acute portal vein thrombosis, systemic sarcoidosis	0 and 5
T3	40-49	m	15	23	39	31	13	25	1.4	77	53	Child B cirrhosis, fundal variceal bleeding, history of successfully treated Hepatitis C	0 and 7
T4	60-69	m	43	58	82	103	61	26	1.4	115	109	Child B NASH cirrhosis, refractory ascites	0
T5	60-69	m	10	27	52	52	13	40	1.2	89	138	Child A alcoholic cirrhosis, refractory ascites	0 and 1
T6	80-89	m	39	46	445	475	22	19	1.2	101	167	Child B cryptogenic cirrhosis, esophageal variceal bleeding	4
T7	60-69	f	43	116	545	232	43	35	1.2	120	114	Child B alcoholic cirrhosis, refractory ascites	23
T8	70-79	m	19	22	50	146	10	34	1.2	89	147	Child A NASH cirrhosis, refractory ascites	45
T9	50-59	m	22	31	44	85	19	37	1.3	102	53	Child A alcoholic cirrhosis, history of successfully treated Hepatitis C, esophageal variceal bleeding	27
T10	30-39	m	64	71	43	158	41	37	1.3	166	94	Child B alcoholic cirrhosis, esophageal variceal bleeding	23
T11	60-69	m	27	41	54	88	25	33	3.3	103	81	Child B cirrhosis, esophageal variceal bleeding, portal vein thrombosis, history of successfully treated Hepatitis C	129
T12	50-59	m	38	63	212	180	19	25	1.3	125	117	Child B alcoholic cirrhosis, esophageal variceal bleeding	0 and 7
T13	60-69	f	17	23	31	58	8	33	1.2	66	47	Child A cirrhosis, esophageal variceal bleeding, history of successfully treated Hepatitis C	0 and 2
T14	70-79	f	19	27	24	65	29	37	1.3	114	94	Child A cirrhosis, esophageal variceal bleeding, history of successfully treated Hepatitis C	46
T15	40-49	m	15	24	132	196	38	27	1.2	91	257	Child B alcoholic cirrhosis, refractory ascites	29
T16	50-59	m	22	23	54	52	18	43	1.2	133	59	Child B NASH cirrhosis, refractory ascites	12
T17	60-69	f	60	95	194	225	160	26	1.5	114	26	Child A NASH cirrhosis, portal vein thrombosis, refractory ascites	59
T18	60-69	m	15	39	114	80	14	34	1.2	83	171	CHILD A NASH cirrhosis, refractory ascites	0 and 2

Supplemental Table 6. Characteristics of IBD patients (see fig. 7 and supplemental fig. 9). Active IBD was defined as symptomatic IBD and/or Calprotectin ≥ 200 µg/g; IBD in remission was defined as asymptomatic IBD and Calprotectin < 200 µg/g. Almost all patients in the "active IBD" and "IBD in remission" groups were treated with biologicals (TNF-α inhibitors or α4β7-integrin inhibitors).

	Patients with active IBD under treatment (n=15)	**IBD patients in remission under treatment (n=9)**	**Patients with active IBD under treatment with oral or intravenous steroids* (n=9)**
Sex (M/F)	10/5	5/4	4/5
Age (years)	39.1 (3.6)	46.1 (6.4)	38.2 (3.6)
Diagnosis (Crohn's C/UC)	6/9	6/3	1/8
Calprotectin (µg/g)	863 (267)	42 (15)	2470 (1072)
Hemoglobin (g/l)	139.6 (4.9)	130.9 (3.4)	123.6 (7.1)
Leukocyte count ($x10^9$/l)	7.3 (0.6)	6.8 (0.6)	8.5 (1.1)
Thrombocyte count ($x10^9$/l)	296.4 (26.7)	252.9 (17.8)	327.9 (26.9)
Albumin (g/l)	41.6 (1.1)	40.9 (1.2)	37.8 (2.6)

Values provided are means (+/- SEM)
Crohn's C: Crohn's colitis; UC: Ulcerative colitis
*used for measurement of D-lactate only (fig. 7G), not included in analysis for fig. 7F, because of interference of steroids with the assay (Ag-presentation to MAIT cells)

SUPPLEMENTAL FIGURES

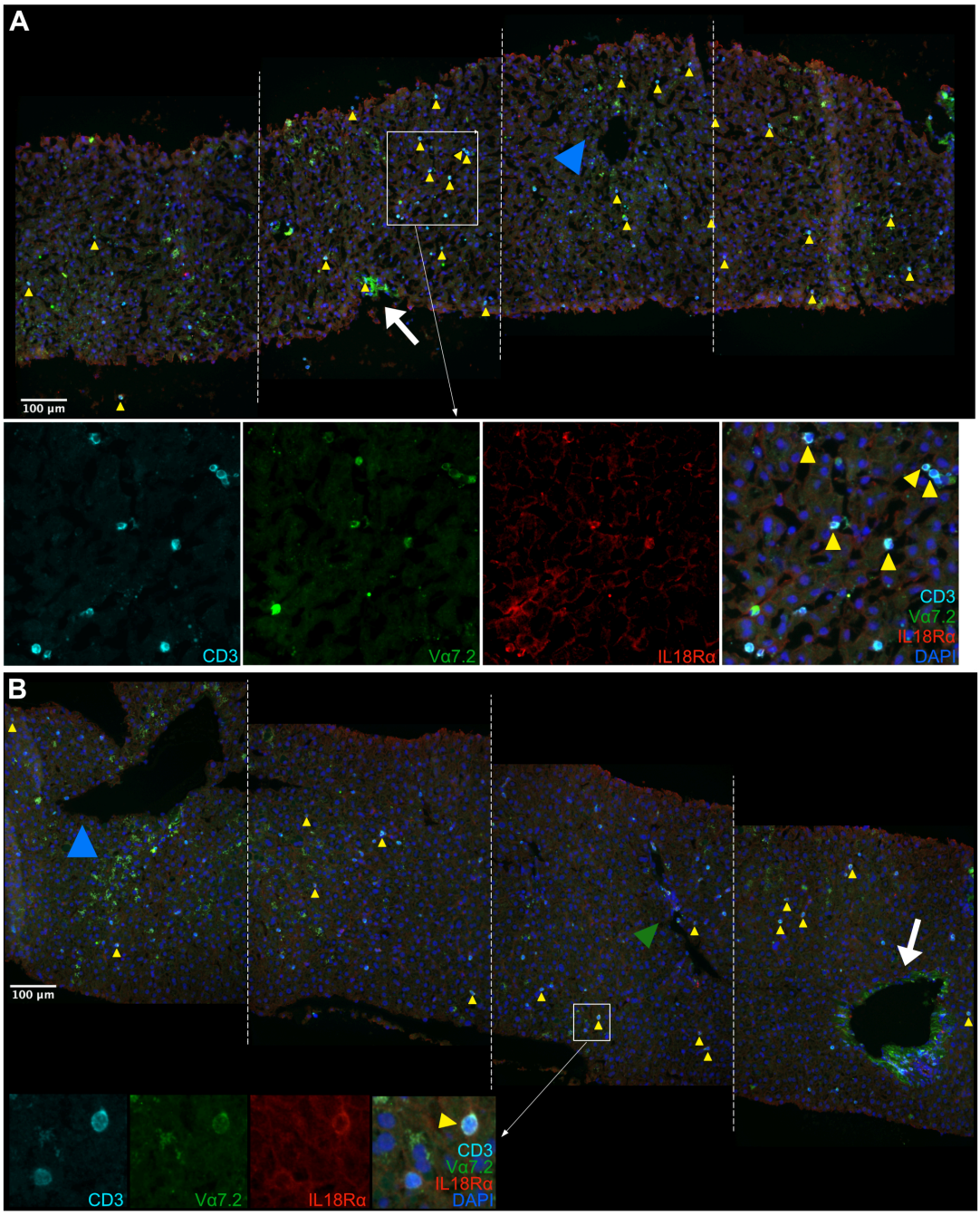

Supplemental Figure 1. Identification of MAIT and NK cells in human liver samples.
(A-B) Dispersed MAIT cell localization in the parenchymal space of normal human liver. Two representative tissue sections from liver biopsies without histopathological abnormalities; patient identifiers C6 (A) and C1 (B). Co-localization of CD3, TCR Vα7.2 and IL-18Rα identifies MAIT cells (yellow arrow heads; see higher magnification lower panels) dispersed within the liver parenchyma. White arrows point towards portal fields, and blue arrow heads towards central veins. The green arrow points to a structure that is likely a central vein. The higher magnification panels also identify MAIT cells in the proximity of T cells negative for IL-18Rα and/or TCR Vα7.2 staining. Abs used for IF staining of cryosections are specified in higher magnification panels.

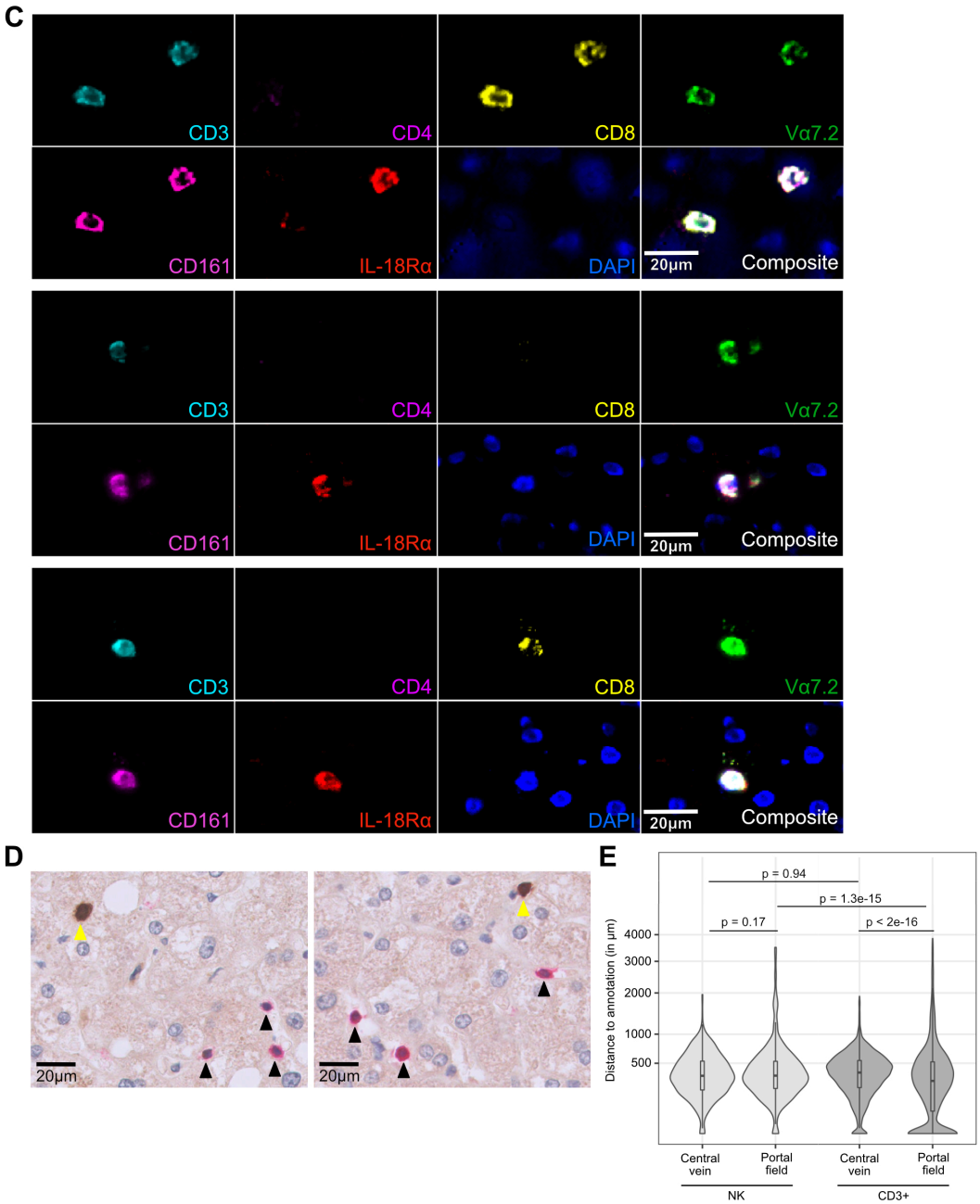

Supplemental Figure 1 (continued). Identification of MAIT cells and NK cells in human liver samples.
(C) IF staining of MAIT cells by chip cytometry using antibodies against CD3, Vα7.2, IL18R-α, CD161, CD4, CD8 and DAPI. Co-localization of CD3, TCR Vα7.2, CD161 and IL-18Rα identifies MAIT cells. The examples show both CD8+ and double negative MAIT cells. (D) Representative examples of CD3 – CD57 double staining (CD3 = red signal, CD57 = brown signal) to detect NK cells (CD3-CD57+) in liver biopsies/resection specimens from patients with normal liver parenchyma. Yellow arrow heads indicate NK cells. Black arrow heads indicate T cells. Scale bars, 20 µm. (E) Violin plot of NK cell and total CD3+ T cell (including MAIT cells) distance to ROIs (portal field and central vein). The box plots indicate the median and quartiles. Data were obtained from analysis of twelve different liver tissues without histopathological abnormalities (4 biopsies and 8 resection specimens). The significance levels were obtained from 1-way ANOVA with selected post-hoc comparisons (t-test), p-values were adjusted with Benjamini-Hochberg correction for multiple testing. The response variable ”distance” was also transformed (square root) to keep also 0 distances in the analysis.

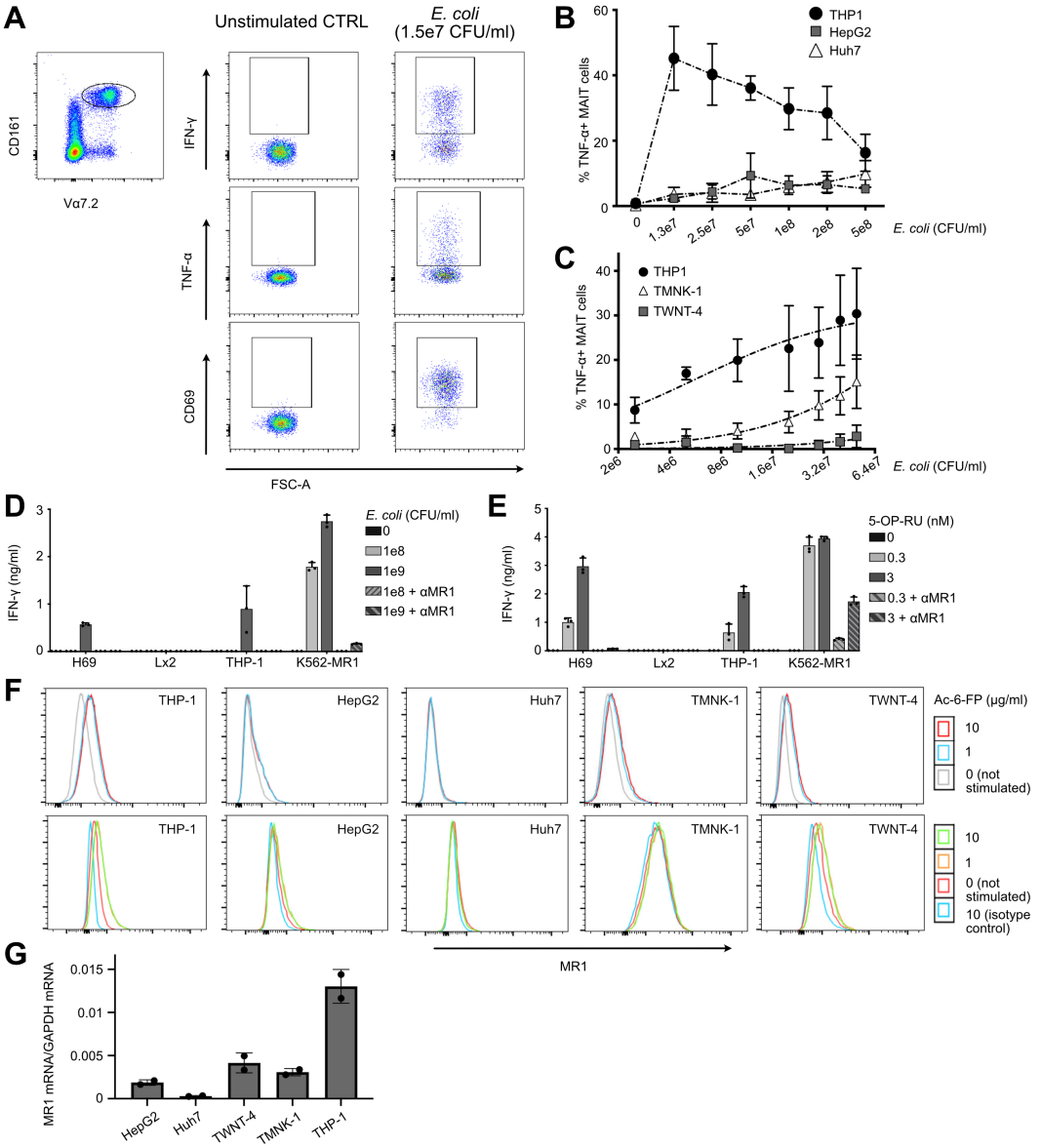

Supplemental Figure 2. Liver-derived established cell lines exert limited capacity to activate MAIT cells.
(A) Characterisation of peripheral blood MAIT cells used in the assays. Representative FACS plot showing MAIT cell identification as $CD161^{++}$ $V\alpha7.2^{+}$ cells within the $CD8^{+}$ cell population (upper left panel). Remaining panels, gated on MAIT cells, represent staining of IFN-γ, TNF-α and CD69 in response to activation by THP-1 cells exposed to fixed *E. coli* (1.5e7 CFU/ml; right panels), compared to unstimulated cells (middle panels; CTRL). (B) Isolated peripheral $CD8^{+}$ T cells co-cultured with THP-1 or hepatoma cell lines exposed to increasing concentrations of fixed *E. coli.* (C) Isolated peripheral $CD8^{+}$ T cells co-cultured with THP-1, LSEC TMNK-1 or stellate TWNT-4 cells exposed to increasing concentrations of fixed *E. coli*. In (B) and (C) TNF-α expression values, measured by FACS, are means ± SD (n = 3). (D and E) SMC3 MAIT cell clone co-cultured with H69 or LX-2 cells exposed to *E. coli* lysate (D) or 5-OP-RU (E), with and without anti-MR1 blocking antibody (αMR1). THP-1 and K562-MR1 cells served as positive controls. IFN-γ secretion values, measured by ELISA, are means + SD from three independent measurements. One representative experiment out of three is shown. (F) FACS histograms showing cell lines (THP-1, HepG2, Huh7, TMNK-1, TWNT-4) stained with anti-MR1 Ab following incubation with no addition, and after addition of 1 or 10 μg/ml of acetyl-6-FP. The lower panels also include staining with an isotype control antibody. (G) RT-qPCR analysis of MR1 mRNA expression in investigated liver cell lines (HepG2, Huh7, TMNK-1, TWNT-4) and control cell line THP-1. MR1 mRNA levels are related to GAPDH mRNA. Results are averages of two independent determinations.

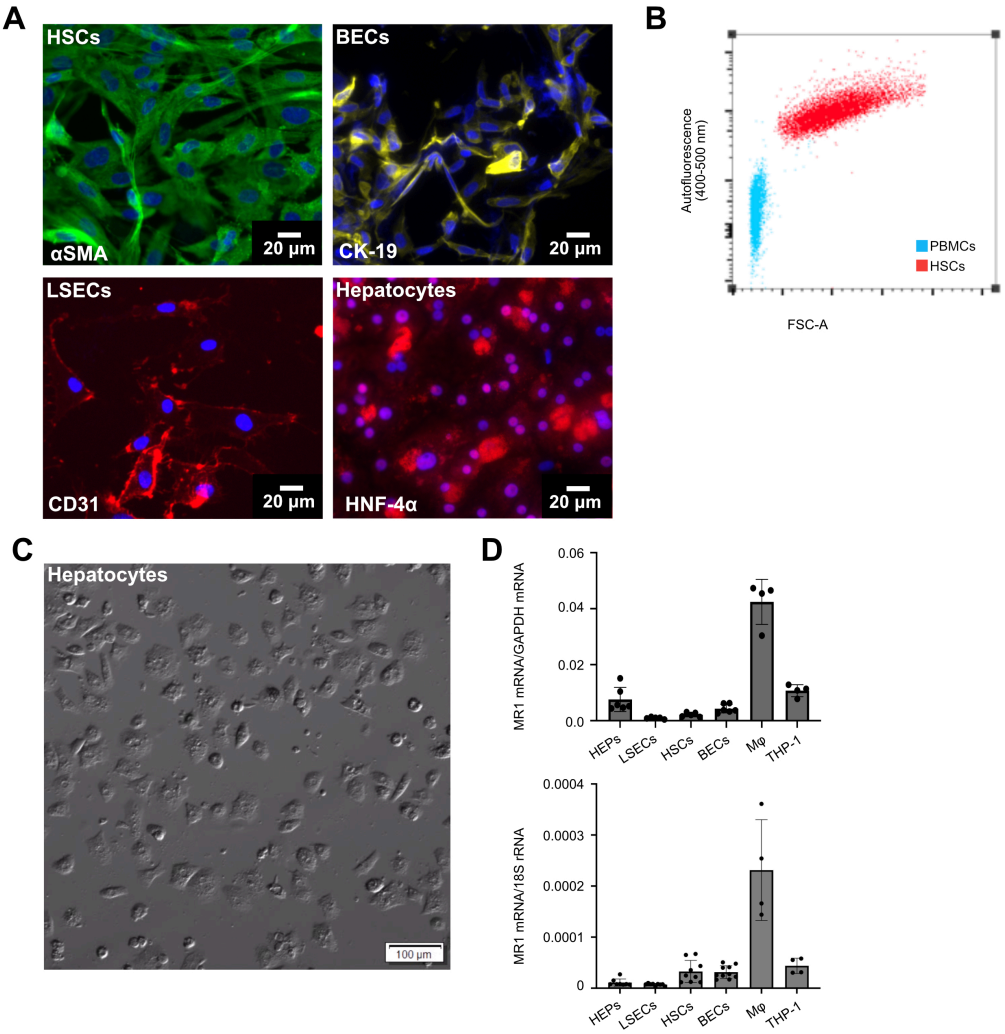

Supplemental Figure 3.
Characterization of primary liver-derived cell subpopulations and their MR1 expression.
(A) Isolated primary cells were analysed by IF for expression of indicated markers. Formalin-fixed cells grown on chamber slides were stained for DAPI, and α-SMA for HSCs, CK-19 for BECs, CD31 for LSECs/liver endothelial cells and HNF-4α for hepatocytes (B) FACS analysis of unstained HSCs compared to human PBMCs. The characteristic autofluorescence of HSCs appears in the violet channel (λ = 400-500 nm). (C) Representative preparation of primary hepatocytes (partially binucleated), used in Ag presentation experiments. The cells were visualized by bright field microscopy. (D) RT-qPCR analysis of MR1 mRNA expression in investigated liver cell subpopulations: hepatocytes/ HEPs, LSECs, HSCs and BECs, and in monocyte-derived macrophages (Mϕ) and THP-1 control cells. MR1 mRNA levels are related to GAPDH mRNA (upper panel) or 18S rRNA (lower panel).

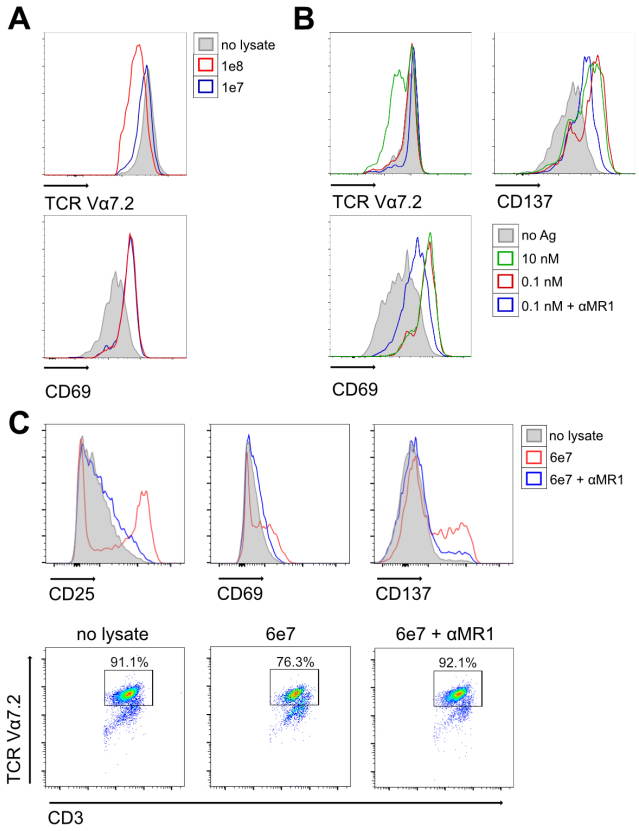

Supplemental Figure 4.
MAIT cell activation in response to Ag-exposed hepatocytes and HSCs.
(A) Representative FACS histograms showing up-regulated activation marker CD69 and down-regulated TCR Vα7.2 on MAIT cell clone SMC3 in response to hepatocytes incubated with *E. coli* lysate (1e7 or 1e8 CFU/ml). (B) Representative FACS histograms showing up-regulated activation markers CD69 and CD137 and down-regulated TCR Vα7.2 on clone SMC3 in response to hepatocytes incubated with 0.1 or 10 nM 5-OP-RU. MR1 dependence of the activation was assessed by the use of anti-MR1 blocking Ab (αMR1). (C) Representative FACS histograms showing up-regulated activation markers CD69, CD25 and CD137 (upper row), and FACS plots (lower row) showing down-regulated TCR Vα7.2, on clone SMC3 in response to HSCs incubated with *E. coli* lysate (6e7 CFU/ml). MR1 dependence of activation was assessed by anti-MR1 blocking Ab.

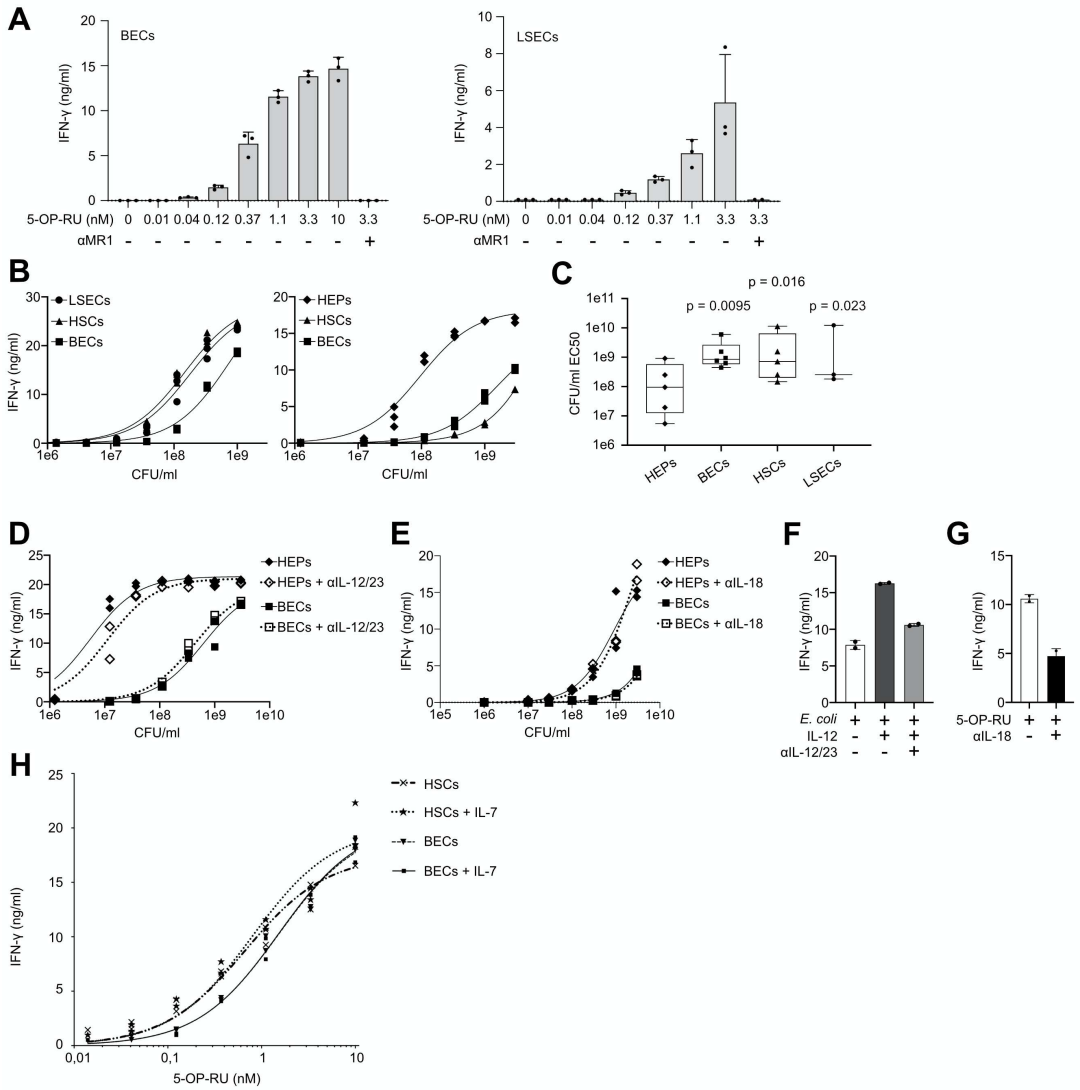

Supplemental Figure 5.
Characterisation of Ag-presentation capabilities of primary liver cells exposed to *E. coli* lysate or 5-OP-RU.
In all panels the IFN-γ production by MAIT cell clone SMC3 was measured by ELISA.
(A) Ag presentation by BECs (left panel) and LSECs (right panel) cells is MR1-dependent. Representative examples of responses to 5-OP-RU at indicated concentrations are shown. Values are means + SD from three independent replicates per dose. (B) Two representative examples of *E. coli* lysate (3e6 - 3e9 CFU/ml) titration using different primary cells (hepatocytes/HEPs, BECs, HSCs, and LSECs) as APCs. Three independent replicates per dose are depicted. (C) Pooled results of all experiments performed as displayed in panel (B). Shown are concentrations of lysate needed to reach EC50 of IFN-γ secretion. P values depict differences between hepatocytes and other APCs as determined by 2-way ANOVA with Dunnet post-hoc test. (D and E) Representative examples of *E. coli* lysate (3e6 - 6e9 CFU/ml) titration using primary hepatocytes/HEPs and BECs as APCs, either in the absence or presence of IL-12/23 (D) or IL-18 (E) blocking Abs. Other details are as in panel (B). (F) Confirmation of blocking efficiency of the anti-IL-12/23 Ab. BECs were stimulated with *E. coli* lysate (1e6 CFU/ml) in the absence or presence of IL-12 and anti-IL-12/23 Ab. (G) Confirmation of blocking efficiency of the anti-IL-18 Ab. THP-1 cells were stimulated with 1 nM 5-OP-RU in the absence or presence of Ab blocking IL-18. (H) Representative example of 5-OP-RU (0.014 - 10 nM) titration using BECs and HSCs as APCs, either in the absence or presence of IL-7.

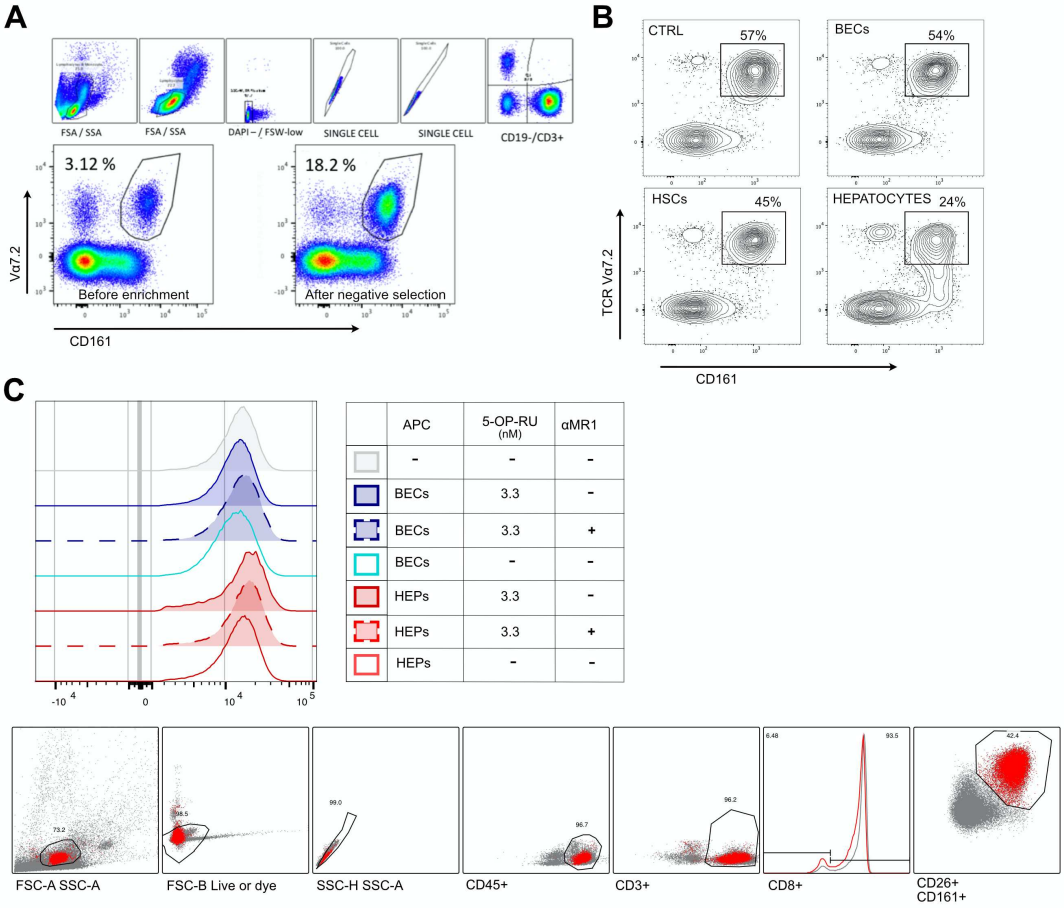

Supplemental Figure 6.
Characterisation of peripheral blood derived MAIT cells.
(A) Representative FACS plot of the MAIT cell population in PBMCs of a healthy donor before and after negative selection with antibodies against CD19, CD45RA, CD14, CD36, CD62L, and TCRγδ. The 5.8-fold enrichment is demonstrated. (B) PBMCs, enriched for Vα7.2^{+} CD161^{++} cells by negative selection (see panel A) were co-cultured with indicated liver APCs exposed to 5 nM 5-OP-RU. Representative example of cell surface expression of CD161 and TCR Vα7.2, as measured by flow cytometry (n = 2). Dot plots are gated on CD3+ cells. (C) CD161 expression on MAIT cells (enriched by negative selection) derived from peripheral blood from a healthy donor is shown. Exact gating strategy for this staining and the experiments depicted in the FACS histograms in the lower panels of Figure 4A is shown (the upper panels in Figure 4A were gated on CD3+CD8+CD26+ cells).

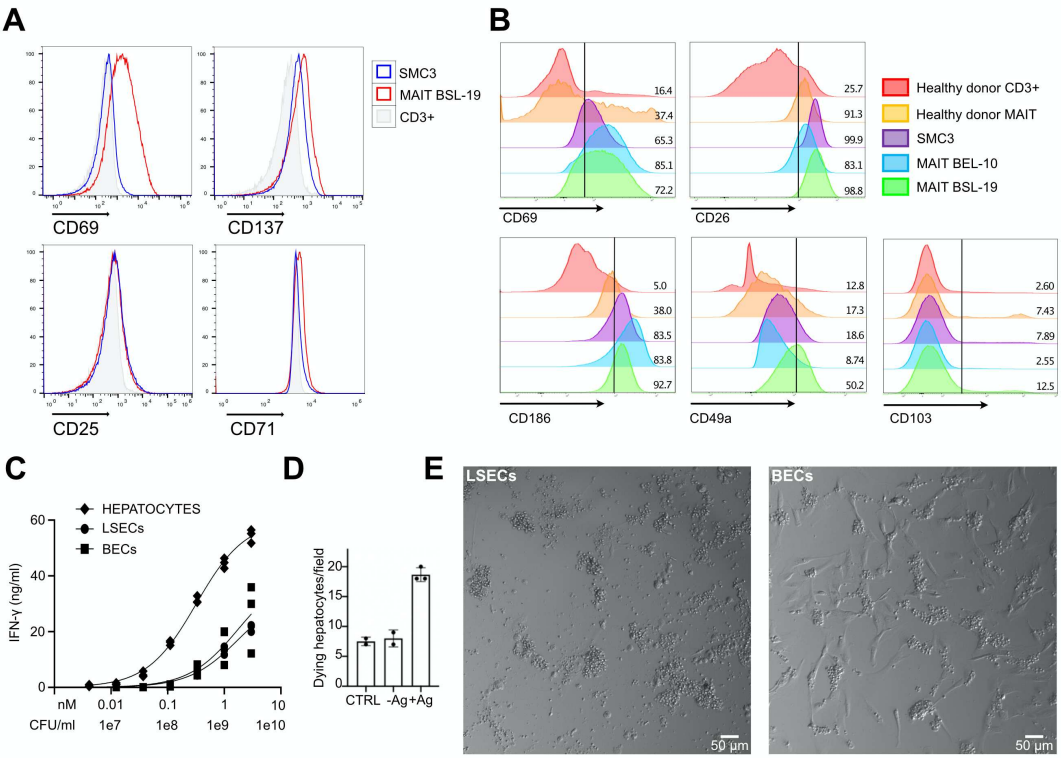

Supplemental Figure 7
Characterisation of liver derived MAIT cell lines BSL-19 and BEL-10 in comparison with other MAIT cell types, and killing potential of MAIT cells (liver derived and clone SMC3) in response to activation by liver APCs.
(A and B) Representative FACS histograms of baseline surface staining of activation, proliferation, and tissue residency markers on liver derived MAIT cell lines BSL-19 (A and B) and BEL-10 (B), on MAIT cell clone SMC3 (A and B), and CD3⁺ (A and B) or MAIT (B) cells derived from peripheral blood of a healthy donor. (C) IFN-γ production by liver-derived MAIT cell line BSL-19, stimulated by indicated liver APCs exposed to increasing concentrations of *E. coli* lysate mixed with 5-OP-RU. Three replicates per dose are shown. (D) Quantification of hepatocyte killing, as visualised by time-lapse microscopy (shown in the Supplementary Videos), by the liver-derived MAIT cell line BSL-19, following activation using mixture of 3 nM 5-OP-RU and 3e9 CFU/ml of *E. coli* lysate (+ Ag). Hepatocytes alone (CTRL) and hepatocytes co-cultured with BSL-19 cells, without any Ag (- Ag), served as negative controls. (E) Representative pictures of LSECs and BECs, exposed to 3 nM 5-OP-RU for 2 h, and then co-cultured with MAIT cell clone SMC3 for 36 h. The LSECs of this patient were very efficiently activating MAIT cell clone SCM3 (corresponding results shown in Fig. 3I, lowest point in the LSEC data), paralleled by an efficient killing of the LSECs. In contrast, most BECs were surviving the co-culture, consistent with a less efficient MAIT cell activation and killing capacity.

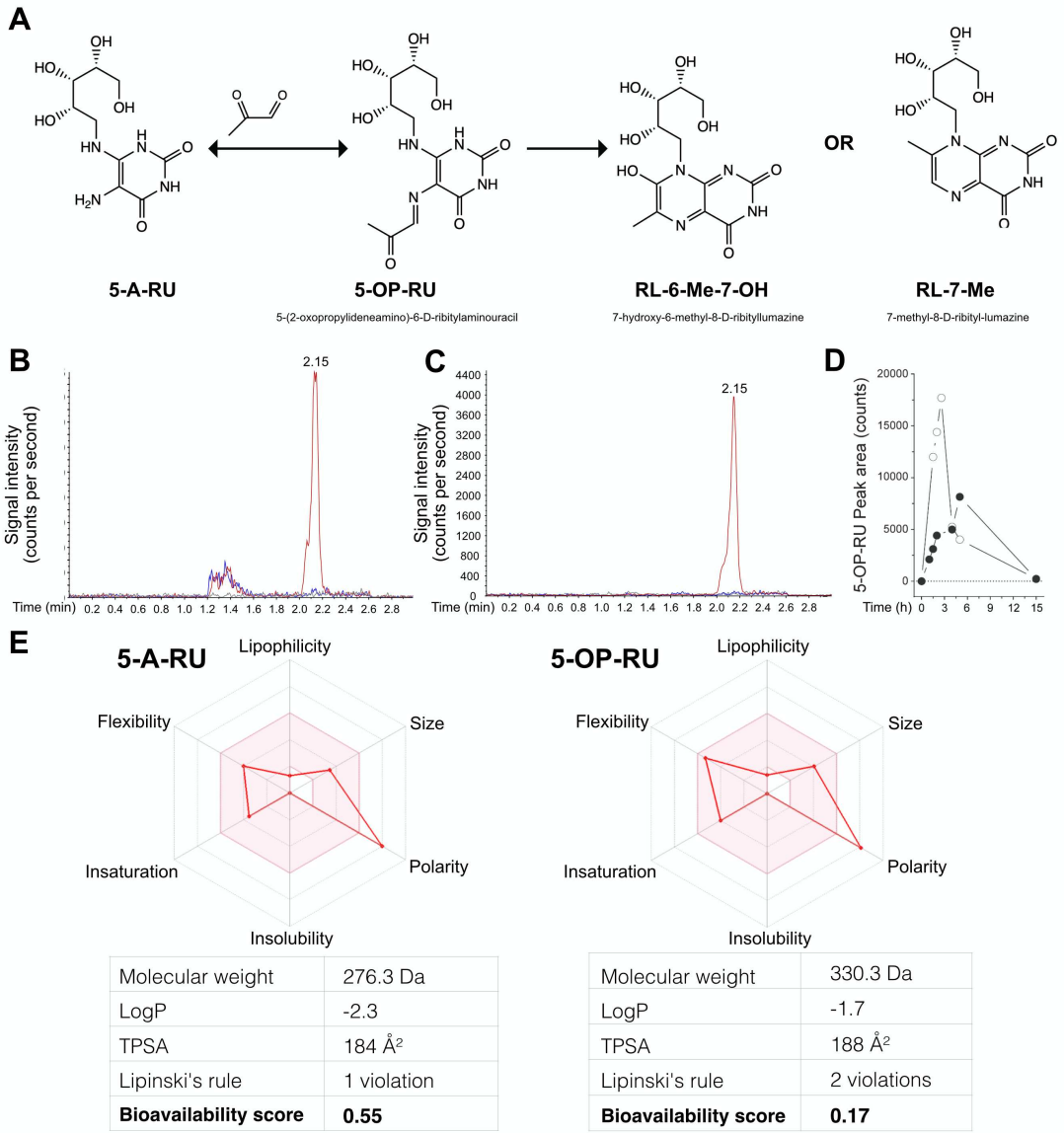

Molecular weight	276.3 Da
LogP	-2.3
TPSA	184 Å²
Lipinski's rule	1 violation
Bioavailability score	**0.55**

Molecular weight	330.3 Da
LogP	-1.7
TPSA	188 Å²
Lipinski's rule	2 violations
Bioavailability score	**0.17**

Supplemental Figure 8.
Scheme of 5-OP-RU formation and its detection by LC-MS/MS, and i*n silico* modeling and bioavailability scores of 5-A-RU and 5-OP-RU.
(A) Scheme of generation of 5-OP-RU from 5-A-RU and methylglyoxal, and of catabolism of 5-OP-RU, adapted from Corbett et al. (17) (B) Overlay of three LC-MS/MS chromatograms identifying 5-OP-RU in lysate of THP-1 cells following incubation with 1 µM 5-A-RU (Red, 5-OP-RU following 5 h incubation; Blue, 5-OP-RU following 15 h incubation; dark grey, pure methanol injection). 5-OP-RU exhibited a retention time of 2.15 min and was detected by selected reaction monitoring in the negative mode (mass transition: 329.0 m/z → 190.9 m/z). (C) Overlay of three LC-MS/MS chromatograms identifying 5-OP-RU in supernatant of THP-1 cells incubated with 1 µM 5-A-RU (Red, 5-OP-RU following 2.6 h incubation; blue, 5-OP-RU following 15 h incubation; dark grey, pure methanol injection). (D) LC-MS/MS analysis of cell extracts and the corresponding culture supernatants following incubation of THP-1 cells with 1 µM 5-A-RU. Shown are time-course accumulation curves of 5-OP-RU in cell lysate (black circles) and cell culture supernatant (open circles). (E) *In silico* modelling was performed by applying a published method,(23,24) using a combination of physicochemical parameters, applied to the Ag 5-OP-RU and its precursor 5-A-RU. We have selected 4 important parameters for display in this figure (molecular weight; LogP, corresponding to the partition coefficient in octanol/water; TPSA, total polar surface area; number of "Lipinski's rule" violations). A higher bioavailability score corresponds to higher probability of intestinal absorption. The score was calculated using an online tool for bioavailability.(25)

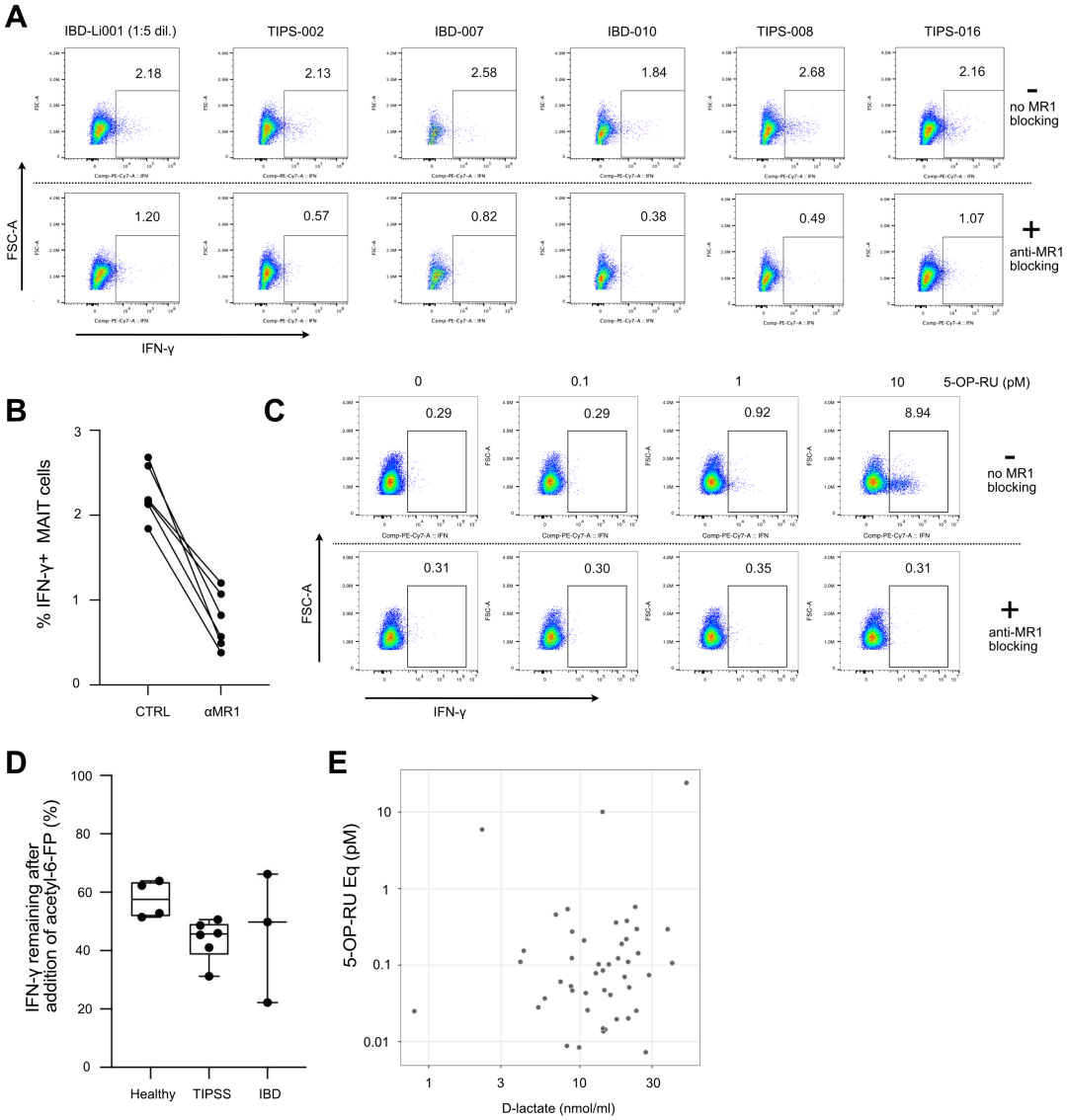

Supplemental Figure 9.
Characterization of MAIT cell responses to stimulatory ligands present in serum of patients with portal hypertension and IBD.
(A-C) FACS analysis reveals MR1-dependent Intracellular IFN-γ staining in SMC3 MAIT cells in response to patient sera or 5-OP-RU. SMC3 cells were stimulated by K562-MR1 cells exposed for 7 h to indicated patient sera (A) or indicated concentrations of 5-OP-RU (C). The graph in (B) represents a summary of the data depicted in (A). In (A) and (C) one experiment of the two performed is shown. (D) Acetyl-6-FP inhibits MAIT cell activation induced by human sera originating from healthy subjects (HEALTHY) as well as those from TIPSS and IBD patients. K562-MR1 cells were incubated with 5 μM acetyl-6-FP for 1 h before the addition of human serum, followed by 3 h incubation before the addition of SMC3 MAIT cells and further incubation for 16 h. Values represent fraction of IFN-γ secretion remaining after addition of acetyl-6-FP. (E) Correlation of serum D-lactate levels with the IFN-γ secretion by MAIT cells (calculated as 5-OP-RU equivalents) in response to stimulation by K562-MR1 cells exposed to human sera from healthy donors, IBD patients and patients with history of TIPSS placement (Spearman correlation coefficient = 0.103).

SUPPLEMENTAL VIDEOS

Supplemental Videos V1-7. Killing efficiency of MAIT cells in response to activation by hepatocytes. Co-culture of hepatocytes with liver-derived MAIT cell line MAIT-BSL-19, using a mixture of 5-OP-RU (3 nM) and *E. coli* lysate (3e9 CFU/ml) as Ags. V1 - V3, cells co-cultured in the presence of Ags (labelled + Ag). V4 and V5, cells co-cultured in the absence of Ags (labelled - Ag). V6 and V7, hepatocytes cultured alone (labelled CTRL). Starting with the addition of MAIT cells to the culture, videos were taken for 15 h. The quantification of hepatocyte killing is shown in supplemental fig. 7D.

Lett MJ, *et al. Gut* 2022;0:1–13. doi: 10.1136/gutjnl-2021-324478

REFERENCES

1. Portmann S, Fahrner R, Lechleiter A, Keogh A, Overney S, Laemmle A, et al. Antitumor effect of SIRT1 inhibition in human HCC tumor models in vitro and in vivo. Molecular cancer therapeutics. 2013;12(4):499-508.
2. Shetty S, Weston CJ, Oo YH, Westerlund N, Stamataki Z, Youster J, et al. Common lymphatic endothelial and vascular endothelial receptor-1 mediates the transmigration of regulatory T cells across human hepatic sinusoidal endothelium. Journal of immunology. 2011;186(7):4147-55.
3. Fabris L, Strazzabosco M, Crosby HA, Ballardini G, Hubscher SG, Kelly DA, et al. Characterization and isolation of ductular cells coexpressing neural cell adhesion molecule and Bcl-2 from primary cholangiopathies and ductal plate malformations. Am J Pathol. 2000;156(5):1599-612.
4. Guven S, Mehrkens A, Saxer F, Schaefer DJ, Martinetti R, Martin I, et al. Engineering of large osteogenic grafts with rapid engraftment capacity using mesenchymal and endothelial progenitors from human adipose tissue. Biomaterials. 2011;32(25):5801-9.
5. Di Maggio N, Mehrkens A, Papadimitropoulos A, Schaeren S, Heberer M, Banfi A, et al. Fibroblast growth factor-2 maintains a niche-dependent population of self-renewing highly potent non-adherent mesenchymal progenitors through FGFR2c. Stem Cells. 2012;30(7):1455-64.
6. Crampton SP, Davis J, Hughes CC. Isolation of human umbilical vein endothelial cells (HUVEC). J Vis Exp. 2007(3):183.
7. Boyum A. Separation of leukocytes from blood and bone marrow. Introduction. Scand J Clin Lab Invest Suppl. 1968;97:7.
8. Schindelin J, Rueden CT, Hiner MC, Eliceiri KW. The ImageJ ecosystem: An open platform for biomedical image analysis. Mol Reprod Dev. 2015;82(7-8):518-29.
9. Bankhead P, Loughrey MB, Fernandez JA, Dombrowski Y, McArt DG, Dunne PD, et al. QuPath: Open source software for digital pathology image analysis. Sci Rep. 2017;7(1):16878.
10. Hagel JP, Bennett K, Buffa F, Klenerman P, Willberg CB, Powell K. Defining T Cell Subsets in Human Tonsils Using ChipCytometry. Journal of immunology. 2021.
11. Correia AL, Guimaraes JC, Auf der Maur P, De Silva D, Trefny MP, Okamoto R, et al. Hepatic stellate cells suppress NK cell-sustained breast cancer dormancy. Nature. 2021;594(7864):566-71.
12. Schmidt U. WM, Broaddus C., Myers G. Cell Detection with Star-Convex Polygons. Springer, Cham. 2018;11071.
13. Stoltzfus CR, Filipek J, Gern BH, Olin BE, Leal JM, Wu Y, et al. CytoMAP: A Spatial Analysis Toolbox Reveals Features of Myeloid Cell Organization in Lymphoid Tissues. Cell Rep. 2020;31(3):107523.
14. Lepore M, Kalinichenko A, Calogero S, Kumar P, Paleja B, Schmaler M, et al. Functionally diverse human T cells recognize non-microbial antigens presented by MR1. Elife. 2017;6.
15. Huang S, Gilfillan S, Cella M, Miley MJ, Lantz O, Lybarger L, et al. Evidence for MR1 antigen presentation to mucosal-associated invariant T cells. J Biol Chem. 2005;280(22):21183-93.
16. Lepore M, Kalinichenko A, Colone A, Paleja B, Singhal A, Tschumi A, et al. Parallel T-cell cloning and deep sequencing of human MAIT cells reveal stable oligoclonal TCRbeta repertoire. Nature communications. 2014;5:3866.
17. Corbett AJ, Eckle SB, Birkinshaw RW, Liu L, Patel O, Mahony J, et al. T-cell activation by transitory neo-antigens derived from distinct microbial pathways. Nature. 2014;509(7500):361-5.
18. Grubman SA, Perrone RD, Lee DW, Murray SL, Rogers LC, Wolkoff LI, et al. Regulation of intracellular pH by immortalized human intrahepatic biliary epithelial cell lines. Am J Physiol. 1994;266(6 Pt 1):G1060-70.
19. Aden DP, Fogel A, Plotkin S, Damjanov I, Knowles BB. Controlled synthesis of HBsAg in a differentiated human liver carcinoma-derived cell line. Nature. 1979;282(5739):615-6.
20. Nakabayashi H, Taketa K, Miyano K, Yamane T, Sato J. Growth of human hepatoma cells lines with differentiated functions in chemically defined medium. Cancer research. 1982;42(9):3858-63.

21. Xu L, Hui AY, Albanis E, Arthur MJ, O'Byrne SM, Blaner WS, et al. Human hepatic stellate cell lines, LX-1 and LX-2: new tools for analysis of hepatic fibrosis. Gut. 2005;54(1):142-51.
22. Matsumura T, Takesue M, Westerman KA, Okitsu T, Sakaguchi M, Fukazawa T, et al. Establishment of an immortalized human-liver endothelial cell line with SV40T and hTERT. Transplantation. 2004;77(9):1357-65.
23. Lipinski CA, Lombardo F, Dominy BW, Feeney PJ. Experimental and computational approaches to estimate solubility and permeability in drug discovery and development settings. Adv Drug Deliv Rev 2001;46:3-26.
24. Martin YC. A bioavailability score. J Med Chem 2005;48:3164-3170.
25. Daina A, Michielin O, Zoete V. SwissADME: a free web tool to evaluate pharmacokinetics, drug-likeness and medicinal chemistry friendliness of small molecules. Sci Rep 2017;7:42717.